



Title	Topology Optimization of Permanent Magnet Synchronous Motor Considering the Control System
Author(s)	Hayashi, Shogo; Kubota, Yoshihisa; Soma, Shingo; Ohtani, Makoto; Igarashi, Hajime
Citation	IEEE transactions on magnetics, 58(9), 8205605 https://doi.org/10.1109/TMAG.2022.3172718
Issue Date	2022-09
Doc URL	http://hdl.handle.net/2115/87019
Rights	© 2022 IEEE. Personal use of this material is permitted. Permission from IEEE must be obtained for all other uses, in any current or future media, including reprinting/republishing this material for advertising or promotional purposes, creating new collective works, for resale or redistribution to servers or lists, or reuse of any copyrighted component of this work in other works.
Type	article (author version)
File Information	hayashi_compumag.pdf



[Instructions for use](#)

Topology Optimization of Permanent Magnet Synchronous Motor Considering the Control System

Shogo Hayashi¹, Yoshihisa Kubota², Shingo Soma², Makoto Ohtani², Hajime Igarashi¹

¹Graduate School of Information Science and Technology, Hokkaido University, Sapporo 060-0814, Japan

²Honda R&D Co., Ltd. Automobile R&D Center, Tochigi 321-3393, Japan

This paper proposes a novel topology optimization approach for permanent magnet synchronous motors (PMSMs) driven by a pulse width modulation (PWM) current control system operating in different modes such as maximum torque per ampere and weakening flux controls. The cost function consisted of iron and copper losses, which are computed considering the spatial and time harmonics in the current generated under these conditions. It is demonstrated that the total loss of the optimized model is reduced compared with that of the conventional model in the operating region.

Index Terms— Behavior model, copper loss, iron loss, permanent magnet synchronous motor (PMSM), topology optimization.

I. INTRODUCTION

IN recent years, permanent magnet synchronous motors (PMSMs) have been extensively used for traction in electric vehicles. Therefore, it is crucial to increase the efficiency of PMSMs to reduce the environmental load and improve machine performance.

The motor structure and control system of PMSM can be optimized to improve its performance. Interior PMSMs consist of permanent magnets inside the rotor. The motor structure of interior PMSM has multiple parameters such as the shape and arrangement of the flux barriers and permanent magnets, and their magnetization directions. These parameters should be optimized to minimize the loss while maintaining high torque characteristics under an assumed control mode.

In the case of conventional topology optimization of motors, e.g., [1], the motor is assumed to be driven by sinusoidal currents, and the spatial and time harmonics are neglected. However, PMSMs are usually driven by pulse width modulation (PWM) inverters that can generate harmonic distortions in the driving current. In this paper, we propose a topology optimization approach for PMSMs driven by a PWM current control system operating in different control modes. So far as the authors know, few studies on such topology optimization have been reported. A high-speed drive simulation based on behavior model [2] is performed for the optimization. The motor state is represented in terms of d- and q-axis fluxes, which are the functions of d- and q-axis currents, and the machine angle. These variables are controlled under different modes suitable for driving conditions. The proposed optimization can be used to enhance the design of PMSMs for electric vehicles and industrial systems.

II. OPTIMIZATION METHOD

A. Topology Optimization

It is crucial to determine the optimum location and design of flux barriers used in a rotor to ensure efficient operation. Therefore, topology optimization is adopted to determine the material distribution without setting the shape parameters.

Various methods are used for topology optimization, which includes sensitivity-based approaches such as the level set method [3],[4] and density method [5], and stochastic approaches based on the Normalized Gaussian Network (NGnet) applied to the ON/OFF method [1], [6]. In this study, the NGnet method was used owing to its high searchability and versatility. In this method, Gaussian basis functions are placed in the design region and the material distribution is determined by the shape function expressed as

$$y(\mathbf{x}, \mathbf{w}) = \sum_{i=1}^N w_i b_i(\mathbf{x}) \quad (1)$$

where w_i is the weighting coefficient, \mathbf{x} is the position vector, and N is the number of Gaussian basis functions. $b_i(\mathbf{x})$ is the normalized Gaussian basis function, which can be expressed as

$$b_i(\mathbf{x}) = \frac{G_i(\mathbf{x})}{\sum_{k=1}^N G_k(\mathbf{x})} \quad (2)$$

$$G_k(\mathbf{x}) = \frac{1}{2\pi\sigma^2} \exp\left[-\frac{\|\mathbf{x} - \boldsymbol{\mu}_k\|^2}{2\sigma^2}\right] \quad (3)$$

where $\boldsymbol{\mu}_k$ and σ^2 are the center of the k th Gaussian basis and variance, respectively. The material attribute v_e of a finite element e can be obtained using

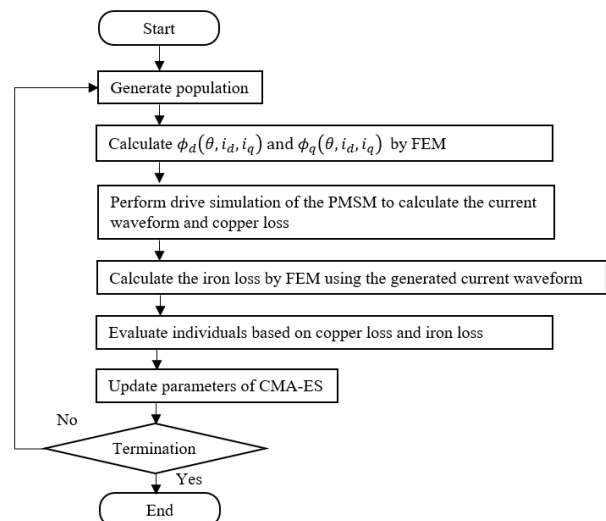


Fig. 1. Flow diagram of the proposed optimization using CMA-ES

$$v_e \leftarrow \begin{cases} \text{air}, & y < 0 \\ \text{iron}, & y \geq 0 \end{cases} \quad (4)$$

The material distribution is dependent upon \mathbf{w} , which is determined to minimize the cost function. Therefore, the topology optimization is reduced to parameter optimization with respect to \mathbf{w} .

B. Flow Diagram of Optimization

The sensitivity of the cost and constraint functions cannot be evaluated with respect to \mathbf{w} . A stochastic algorithm was used because it does not require sensitivity values to determine \mathbf{w} . Stochastic optimization is performed using finite element analysis to evaluate individuals. In this work, covariance matrix adaptation evolution strategy (CMA-ES) [7] was adopted for the stochastic algorithm. The number of individuals required for search increases only in $O(\log N)$, while that for the genetic algorithm increases in $O(N)$, where N represents the number of variables (here, basis functions). In CMA-ES, the individuals are generated according to the mean vector and covariance matrix, which are adaptively changed during the optimization. The flow diagram of the optimization using CMA-ES is shown in Fig. 1.

C. Drive System

PMSMs are usually driven by inverters, which generate time harmonics in the current. For the input PWM voltage, the current wave is determined by solving the voltage equation. The control system used for the optimization is represented by the block diagram shown in Fig. 2. The current command is generated from the torque command and the rotation speed. The current command is generated under maximum torque per ampere (MTPA) control or flux-weakening control. The latter is operated to decrease the back EMF lower than that of the supply voltage of the inverter. Control Unit 1 provides Control Unit 2 with the voltage command through proportional integral (PI) control. Subsequently, Control Unit 2 generates the series of PWM voltages, which are input to the motor plant model,

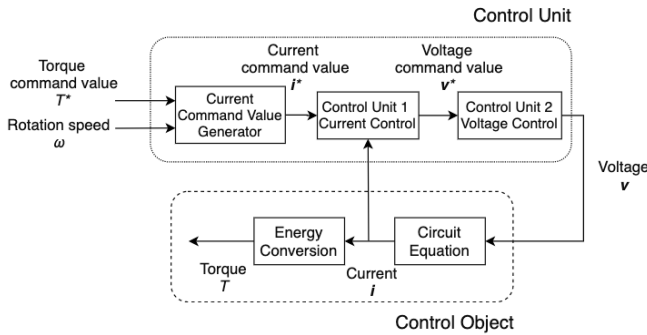


Fig. 2. Block diagram of the controller

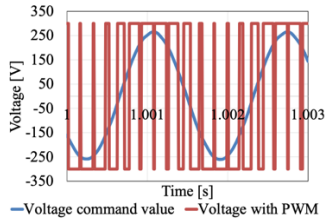


Fig. 3. Voltage waveform

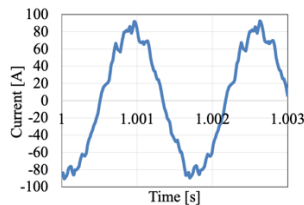


Fig. 4. Current waveform

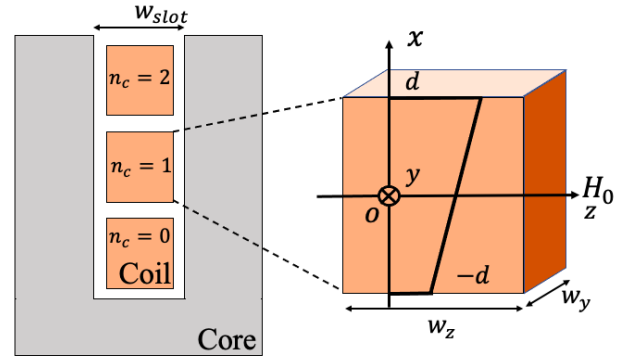


Fig. 5. Simplified model and distribution of the external magnetic field inside the coil

and the current waveform is obtained by solving the voltage equation. Finally, the current is input to Control Unit 1 and is used to compute the torque. The generated PWM voltage and corresponding current waves are plotted in Figs. 3 and 4.

D. Loss Calculation

It is necessary to compute iron and copper losses to evaluate the total loss. The losses should be quickly evaluated during the optimization process. The iron losses in the stator and rotor cores are evaluated using the measured loss density of the electromagnetic steel sheet p_{iron} , which is the function of frequency f and the magnitude of magnetic induction B . It is expressed as:

$$P_{iron} = \sum_e \sum_i p_{iron}(f_i, B(e, i)) \cdot v_e \quad (5)$$

where f_i is the i -th harmonic frequency, $B(e, i)$ is the i -th Fourier component of the magnetic flux density of the e -th finite element with a volume v_e .

The DC and AC losses generated in the coils are determined to calculate the copper losses, which is simplified as shown in Fig. 5. It is assumed that the permeability of the iron core, length of the coil in the axial direction, and the width w_z of the coil are adequate. Therefore, the magnetic field enters in a perpendicular direction to the coil surfaces and only H_z remains. The external magnetic field H_0 is assumed to have a linear distribution in x direction as shown in Fig. 5. The 1D quasi-static field equation are solved using these assumptions. It was observed that the copper loss in the coil P_{copper} can be expressed as:

$$P_{copper}(t) = \frac{dw_y w_z}{\sigma} \left(2J_0^2(t) + \sum_n F_{h,n}^2(t) + \sum_n F_{l,n}^2(t) \right) \quad (6a)$$

$$F_{h,n} = \frac{2}{d} \cos\left(\frac{n\pi}{2}\right) \int_{-\infty}^t \left(e^{n^2 K^2 D(\tau-t)} \frac{d \sum_{k=0}^{n_c} i_k(\tau) - \sum_{k=-1}^{n_c-1} i_k(\tau)}{2w_{slot}} \right) dt \quad (6b)$$

$$F_{l,n} = \frac{2}{d} \sin\left(\frac{n\pi}{2}\right) \int_{-\infty}^t \left(e^{n^2 K^2 D(\tau-t)} \frac{d \sum_{k=0}^{n_c} i_k(\tau) + \sum_{k=-1}^{n_c-1} i_k(\tau)}{2w_{slot}} \right) dt \quad (6c)$$

where d , w_y , and w_z denote the coil sizes defined in Fig.5. w_{slot} is the slot width, σ and μ are the electrical conductivity

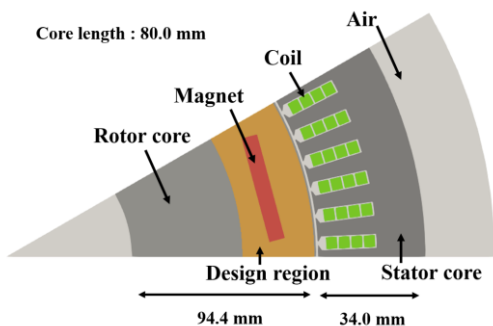


Fig. 6. Optimization model

TABLE I Motor specifications

Phases and poles	3 phases, 12 poles
Coil Turns	4
Number of stator slots	72
Residual flux density	1.1 T
Electromagnetic Steel Sheets	35JN270

TABLE II Inverter specifications

Current	250 A
Voltage	600 V
Carrier Frequency	6000 Hz

TABLE III Settings of CMA-ES

Number of generations	50
Number of genes	39
Size of population	64

TABLE IV Settings of the reference table and FEM

Machine angle for table data	0.000, 1.000, ..., 10.00 deg
d-axis current for table data	-150.0, -112.5, ..., 0.000 A
q-axis currents for table data	0.000, 37.50, ..., 150.0 A
Number of FEM analyses required to create table data	275
Number of FEM analyses required for iron loss analysis	98

and permeability, respectively. J_0 is the external current. i_k is the k -th Fourier component of the current, where $i_{-1} = 0$ and $K = \pi/2d$, $D = 1/\sigma\mu$.

III. OPTIMIZATION RESULTS

A. Optimization Setting

The rotor shape was determined using topology optimization to reduce the losses. The optimization model is shown in Fig. 6, and the specifications of the motor and inverter are summarized in TABLE I and II. The cost function consists of the iron loss P_{iron} and copper loss P_{copper} evaluated under the two different control modes. The MTPA control (mode 1) and weakening flux control (mode 2) were performed for each control mode. The optimization problem is defined as:

$$\text{minimize } F(\mathbf{w}) = \sum_{i=1}^2 \frac{1}{2} \left(\frac{3 P_{i,iron}}{4 P_{i,iron}^{ref}} + \frac{1 P_{i,copper}}{4 P_{i,copper}^{ref}} \right) \quad (7)$$

where index i represents the control mode. $P_{i,iron}^{ref}$ and $P_{i,copper}^{ref}$ are the iron and copper losses of the reference model shown in Fig. 7 for each control mode. The rotational speed and torque command values for mode 1 were set to 2000 rpm and 125 Nm, respectively, whereas the rotational speed and torque command values for mode 2 were set as 6000 rpm and 75 Nm,

respectively.

TABLE III and IV summarize the settings of CMA-ES and the table data referred in the control simulation using the block diagram, respectively. We assumed the values recommended in [7] for the hyperparameters of CMA-ES except the size of population.

B. Optimization result

The resultant rotor shape is shown in Fig. 8. The characteristics of the reference and optimized models are summarized in TABLE V, from which it is concluded that the optimization reduced the total loss by 2.0% in control mode 1 and 14.9% in model 2 compared with those of the reference model. In particular, the iron loss in control mode 2 was reduced by 21% through the optimization. The resultant speed-torque curve is plotted in Fig. 9. Figs. 10 and 11 depict the frequency components of the iron loss and the change in magnetic flux density in the teeth under control mode 2. In the optimized motor, the third-order component of the iron loss was reduced by 83.0%. Additionally, the change in the magnetic flux density demonstrated that the low-frequency component was reduced. Fig. 12 represents the magnetic flux lines in the optimized and reference motors when the difference in the distribution of magnetic induction was large. The rotor surface region was deeply saturated in the optimized motor. This weakened the magnetic flux in the teeth, which reduced the iron loss.

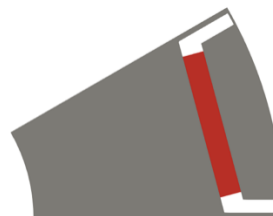


Fig. 7. Reference rotor shape

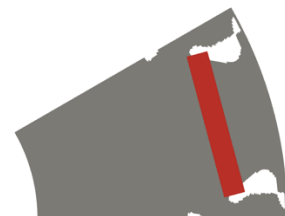


Fig. 8. Resultant rotor shape

TABLE V Characteristics of the reference model and optimized model

	Operation condition 1, 2000 rpm, 125 Nm			Operation condition 2, 6000 rpm, 75 Nm		
	Copper loss [W]	Iron loss [W]	Total loss [W]	Copper loss [W]	Iron loss [W]	Total loss [W]
Reference model	315.7	314.9	630.6	754.8	1126.7	1882
Optimized model	315.9	302.3	618.2	756.5	844.3	1600

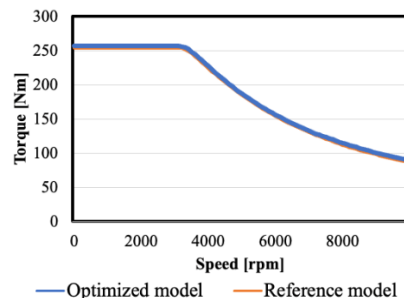


Fig. 9. Speed-torque curves before and after the optimization. The torque characteristics remain unchanged by the optimization, while the loss is reduced.

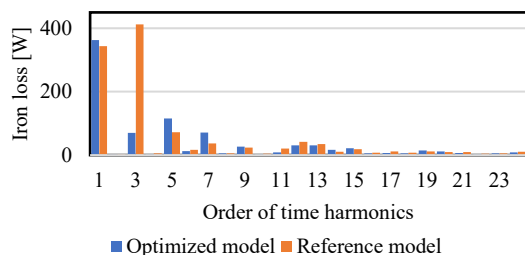


Fig. 10. Frequency components of iron loss

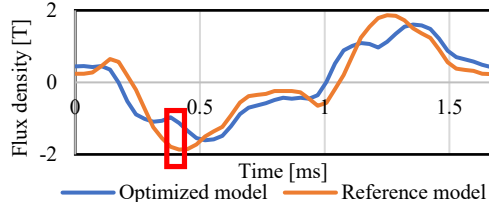


Fig. 11. Change in magnetic flux density at a point in the teeth

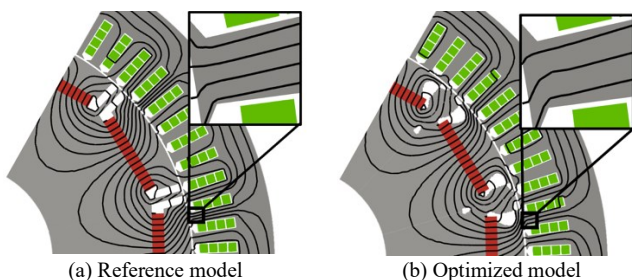


Fig. 12. Magnetic flux line

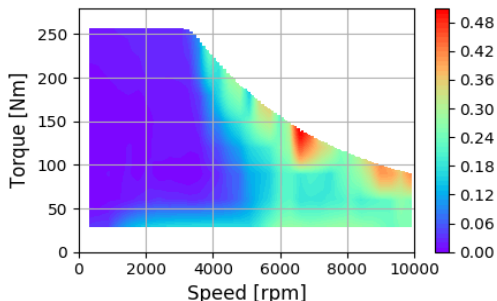


Fig. 13. Loss reduction rate

The loss reduction rate was used to compare the total losses of the motors. The loss reduction rate can be expressed as:

$$\epsilon = \frac{P^{ref} - P^{opt}}{P^{ref}}$$

where P^{ref} and P^{opt} denote the total losses of the reference and optimized motors, respectively. Fig. 13 shows the distribution of ϵ in the operating region. It can be observed that the value of ϵ is positive, which indicated that the value of P^{opt} was smaller than that of P^{ref} over the operating region.

Finally, the cause of the enhanced performance of the optimized core was determined by modifying the core shapes as shown in Fig.14. The flux barrier appears converged near the rotor surface in Fig.14(b). Conversely, in Fig. 14(c), the flux barrier appears expanded. The resultant characteristics are summarized in TABLE VI. In the case of modified model A, the d-axis inductance decreased because the flux circulation around the magnet end was caused by filling the flux barrier. This increased the copper loss under the MTPA control because the current was increased to maximize the torque. Conversely, in the case of modified model B, the loss in the MTPA control

was reduced due to the increased d-axis inductance, whereas the loss in the weakening flux control increased due to the increase in the d-axis current. Therefore, it can be concluded that the optimized core shape provided a good balance between the reduction of total loss under the control modes.

IV. CONCLUSION

A topology optimization approach considering the control system was proposed. The loss was evaluated considering the harmonics in the driving current generated by a PWM inverter. The loss of the PMSM was reduced under the MTPA and weakening flux controls, which were the main control modes.

ACKNOWLEDGMENT

This work was supported in part by the Grants-in-Aid for Scientific Research (KAKENHI) through the Japanese Society for the promotion of Science (JSPS) under Grant 21H01301.

REFERENCES

- [1] T. Sato, K. Watanabe, and H. Igarashi "Multimaterial topology optimization of electric machines based on normalized Gaussian network," *IEEE Trans. Magn.*, vol 51, no. 3, Mar. 2015
- [2] H. Kaimori and K. Akatsu, "Behavior modeling of permanent magnet synchronous motors using flux linkages for coupling with circuit simulation," *IEEJ J. Industry Applications*, vol.7, no.1, 56-63, 2018.
- [3] J. Lee and S. Wang, "Topological shape optimization of permanent magnet in voice coil motor using level set method," *IEEE Trans. Magn.*, vol. 48, no. 2, pp. 931–934, Feb. 2012
- [4] Y. Yamashita and Y. Okamoto, "Design optimization of synchronous reluctance motor for reducing iron loss and improving torque characteristics using topology optimization based on the level-set method," *IEEE Trans. Magn.*, vol. 56, no. 3, pp. 1–4, Mar. 2020
- [5] F. Guo and I. P. Brown, "Simultaneous magnetic and structural topology optimization of synchronous reluctance machine rotors," *IEEE Trans. Magn.*, vol. 56, no. 10, pp. 1–12, Oct. 2020
- [6] H. Sasaki and H. Igarashi, "Topology optimization using basis functions for improvement of rotating machine performances," *IEEE Trans. Magn.*, vol. 54, no. 3, pp. 1–4, Mar. 2018
- [7] N. Hansen, "The CMA evolution strategy: A tutorial," arXiv:1604.00772, 2016.



Fig. 14. Flux barrier in the optimized and modified models.

TABLE VI Characteristics of the optimized model and modified models

	Operation condition 1, 2000 rpm, 125 Nm			Operation condition 2, 6000 rpm, 75 Nm		
	Copper loss [W]	Iron loss [W]	Total loss [W]	Copper loss [W]	Iron loss [W]	Total loss [W]
Optimized model	315.9	302.3	618.2	756.5	844.3	1601
Modified model A	349.3	307.9	657.3	734.6	1010	1745
Modified model B	305.9	301.9	607.8	790.1	921.8	1712